

# Carbon–Silicon Core–Shell Nanowires as High Capacity Electrode for Lithium Ion Batteries

Li-Feng Cui, Yuan Yang, Ching-Mei Hsu, and Yi Cui\*

Department of Materials Science and Engineering, Stanford University,  
Stanford, California 94305

Received May 27, 2009; Revised Manuscript Received July 2, 2009

## ABSTRACT

We introduce a novel design of carbon–silicon core–shell nanowires for high power and long life lithium battery electrodes. Amorphous silicon was coated onto carbon nanofibers to form a core–shell structure and the resulted core–shell nanowires showed great performance as anode material. Since carbon has a much smaller capacity compared to silicon, the carbon core experiences less structural stress or damage during lithium cycling and can function as a mechanical support and an efficient electron conducting pathway. These nanowires have a high charge storage capacity of  $\sim 2000$  mAh/g and good cycling life. They also have a high Coulmbic efficiency of 90% for the first cycle and 98–99.6% for the following cycles. A full cell composed of  $\text{LiCoO}_2$  cathode and carbon–silicon core–shell nanowire anode is also demonstrated. Significantly, using these core–shell nanowires we have obtained high mass loading and an area capacity of  $\sim 4$  mAh/cm<sup>2</sup>, which is comparable to commercial battery values.

Lithium ion batteries that were mainly used for portable electronic devices are now extended to applications such as power tools and electric vehicles. Finding new electrode material with higher capacity or higher energy density has been one of the most important research focuses. Silicon is an attractive alloy-type anode material because of its highest known capacity (4,200 mAh/g). However lithium insertion into and extraction from silicon are accompanied by a huge volume change (up to 300%), which induces a strong stress on the silicon particles and causes pulverization and rapid capacity fading.<sup>1</sup> To overcome this issue, several approaches have been suggested, which includes the preparation of nanosize active materials,<sup>2–7</sup> active/inactive composite materials<sup>8–10</sup> and Si-based carbon composites.<sup>10–15</sup> These approaches have resulted in improvements of the electrochemical performance of Si-based anodes but only to limited extent.

Recently, we developed an approach using Si nanowires (SiNWs) as anodes, which represents one of the most promising solutions.<sup>16–18</sup> We have demonstrated excellent performance of crystalline SiNW anodes directly grown onto stainless metal current collector by a vapor–liquid–solid growth.<sup>16</sup> SiNWs can relax the strain and overcome the problem of pulverization, maintain direct electrical connection with current collector, and have short diffusion distance for lithium insertion. We have also carried out detailed

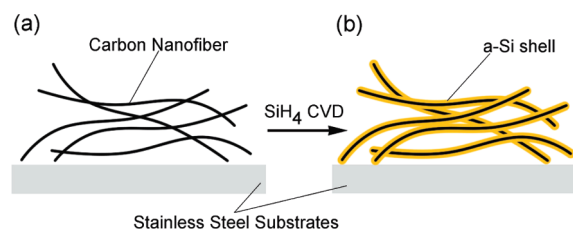


**Figure 1.** Schematic illustration of Si coating onto carbon nanofibers (a) Bare CNFs. (b) C–Si core–shell NWs.

investigations on SiNWs' structural change and solid electrolyte interphase (SEI) during lithium intercalation.<sup>19,20</sup> Following our work, several groups have also reported anode study using SiNWs.<sup>21,22</sup> Furthermore, we have also demonstrated anodes based on crystalline–amorphous core–shell SiNWs<sup>17</sup> directly grown on metal current collectors. By limiting the charging potential above 150 mV versus lithium metal, we have shown that amorphous shell can be selectively used for lithium ion storage with capacity of  $\sim 1000$  mAh/g while crystalline cores remain intact and function as efficient electron transport pathways and stable mechanical support. The crystalline–amorphous core–shell structure further improved the high power performance and the cycle life. In this report, we have synthesized C–Si core–shell NWs by chemical vapor deposition (CVD) of amorphous Si (a-Si) onto carbon nanofibers (CNFs) as illustrated in Figure 1. Their excellent electrochemical performance is also demonstrated. Similar to crystalline Si core in the crystalline–amorphous core–shell SiNWs, carbon cores function as efficient

\* To whom correspondence should be addressed. E-mail: yicui@stanford.edu.

electron transport pathways and stable mechanical support. However, the difference is that the carbon core, due to its small capacity, has little structure or volume change with charge potential down to 10 mV versus lithium metal. Charging to this low potential allows a much higher usage (>2000 mAh/g) of the specific charge capacity of a-Si. In addition, CNFs are commercially available in a large quantity, which makes the mass production of C–Si core–shell NWs easily achievable. We demonstrated the high mass loading of these core–shell NWs and achieved an area capacity of  $\sim 4$  mAh/cm<sup>2</sup>, which is comparable to commercial values.

CNFs were purchased from Sigma-Aldrich and used as obtained. The deposition of CNFs on SS foil substrates was done by drop-cast method or slurry spreading method. For the drop-cast method, CNFs were well dispersed in isopropanol first then deposited on a heated SS substrates (1 cm<sup>2</sup>  $\times$  1 cm<sup>2</sup>) by drop casting from a pipet. A CNF film of loading density up to 0.4 mg/cm<sup>2</sup> can be achieved using this method. After drying, the CNF loaded SS substrates were put inside a SiH<sub>4</sub> CVD furnace for Si coating. For the slurry spreading method, CNFs were mixed with polyvinylidene fluoride (PVdF, 10% weight) in *N*-methylpyrrolidone (NMP) to form slurry and then spread onto a SS foil using an applicator. After drying, the SS foil coated with the CNFs-PVdF film was cut into small pieces (1 cm<sup>2</sup>  $\times$  1 cm<sup>2</sup>) and put inside the CVD furnace. First, the PVdF polymer was decomposed inside the furnace under vacuum and Ar flow at a high temperature of 700 °C for 1 h. After the decomposition of PVdF, the temperature was lowered to 500 °C and SiH<sub>4</sub> was delivered for the Si coating. Using this slurry spreading technique, a relatively uniform film of CNFs with loading density up to 2 mg/cm<sup>2</sup> can be obtained.

Silicon coating on the carbon nanofibers (CNFs) was done using SiH<sub>4</sub> CVD (see Supporting Information, Materials and Methods). After the Si coating, the SS substrates can function directly as current collectors and the C–Si core–shell NWs are the active material for which no binding or conductive additives are needed. Although the CNFs are not directly grown from the SS substrate (current collector), they are conducting themselves and are electrically connected to the SS substrate. After the CVD process, the NW film sticks to the substrate quite well and does not easily delaminate from the SS substrate. Our excellent battery measurements also indicate that a good electrical contact between the NWs and the SS substrates was formed after a-Si deposition. We found that at CVD temperature of 500 °C, a-Si can be selectively deposited onto the CNFs from silane decomposition. To prove that this is a selective deposition, we also put a bare SS substrate (control substrate) in the furnace and very little Si deposition was found on the bare SS substrate. In this study, we did not see much Si crystalline–amorphous core–shell NWs grown on the SS steel substrate, as observed in our previous study,<sup>17</sup> because lower partial pressure and flow rates of SiH<sub>4</sub> were used in this report.

In Figure 2 panels a and b are the scanning electron microscopy (SEM) images of the bare CNFs and Si coated CNFs, respectively. After the Si coating, the diameter of

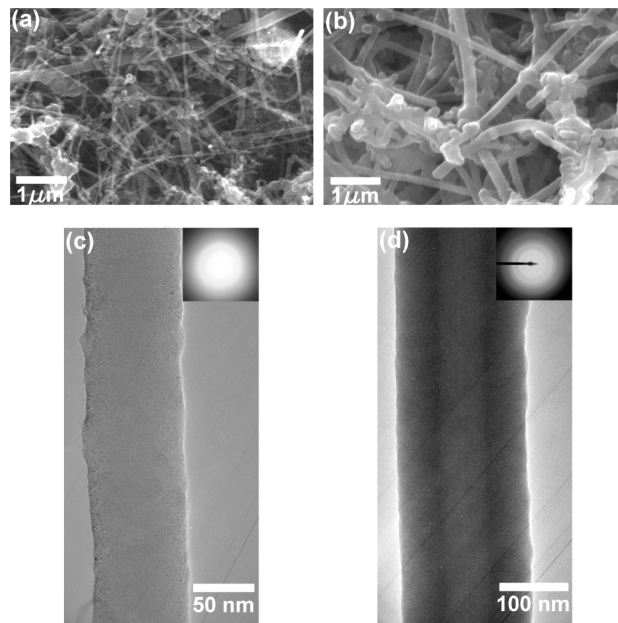


**Figure 2.** (a) SEM image of CNFs before Si coating. (b) SEM image of Si coated CNFs. (c) TEM and SAED images (inset) of a bare CNF. (d) TEM and SAED images (inset) of a C–Si core–shell NW.

CNFs became significantly larger, suggesting a thick layer of Si coating. The bare CNFs obtained from Sigma-Aldrich are amorphous carbon NWs as indicated by the TEM image and the electron diffraction pattern in Figure 2c. After the Si coating, a core–shell structure can be identified by contrast in the TEM image shown in Figure 2d, where the Si shell thickness is  $\sim 50$  nm. Electron diffraction (Figure 1d inset) suggests that the coated Si shell is also amorphous. Energy dispersive spectroscopy (EDS) analysis (Supporting Information, Figure S1) finds dominant Si and C signals and little oxygen signal was observed, indicating little silicon oxides in the Si shell.

The amount of Si deposited is controlled by the SiH<sub>4</sub> CVD time. We controlled the Si/C ratio at  $\sim 3:1$ . The C–Si core–shell NWs were assembled into pouch cells with Li or LiCoO<sub>2</sub> as counter electrode (see Supporting Information, Materials and Methods). No binders or conducting carbon were used. The pouch cells were investigated using galvanostatic charge/discharge.

Figure 3a shows the cycling performance of a-Si coated CNFs, that is, C–Si core–shell NWs. CNFs ( $\sim 0.4$  mg) were drop-casted on to a SS current collector (1 cm<sup>2</sup>  $\times$  1 cm<sup>2</sup>), then a-Si was deposited onto the CNFs using the SiH<sub>4</sub> CVD method to produce C–Si core–shell NWs. The weight of Si deposited was about 3 times of that of CNFs. The obtained NW/SS product was directly used as an electrode and cycled between 1 and 0.01 V versus a Li counter electrode. A very good first cycle Coulombic efficiency of  $\sim 90\%$  was achieved, which is similar to commercial graphite anodes. At the rate of C/5 (1C = 2.5A/g), a reversible capacity of  $\sim 2000$  mAh/g was observed for the first 30 cycles. After the first cycle, the cell maintained a very high Coulombic efficiency between 98–99.5% for the rest of 55 cycles.

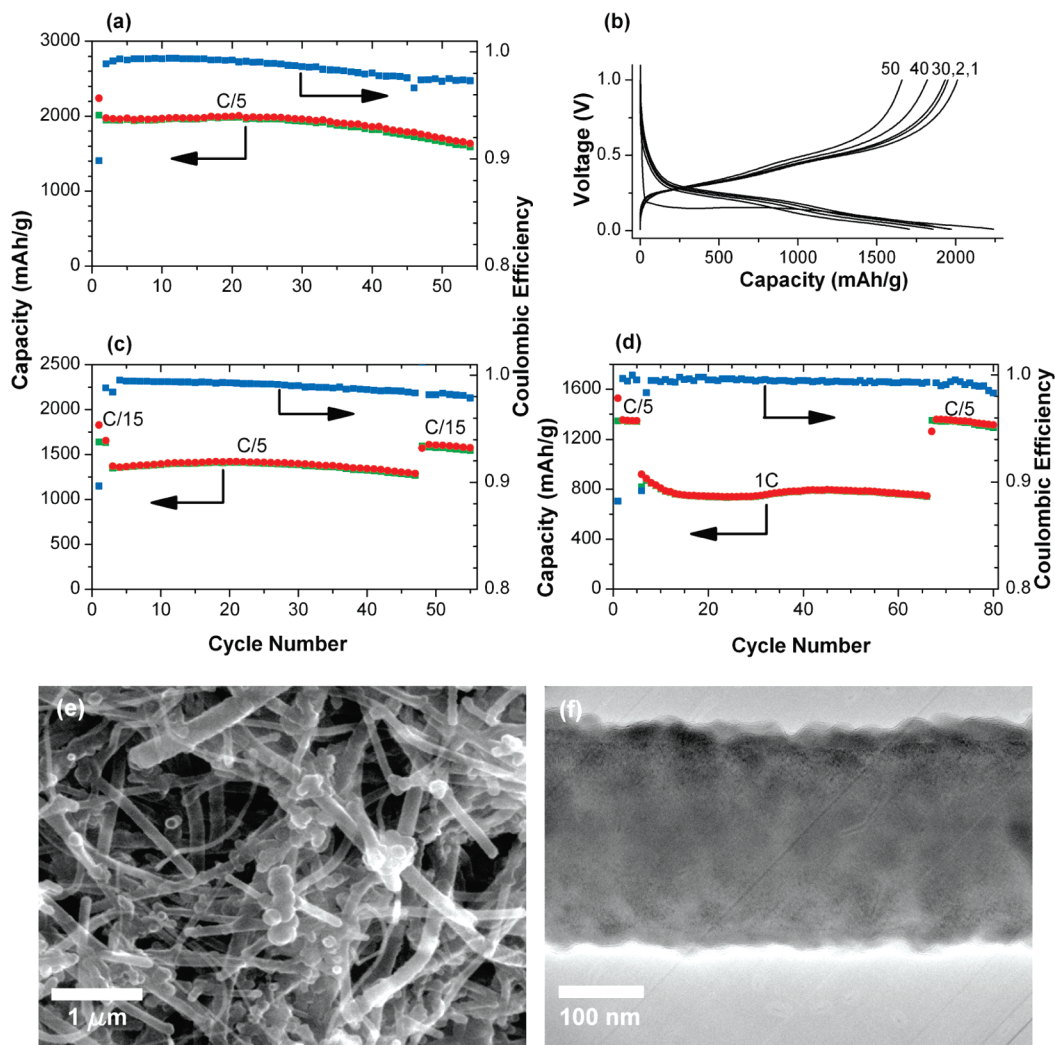


**Figure 3.** (a) Charge (red) and discharge (green) capacity and Coulombic efficiency (blue) versus cycle number for a half cell cycled between 1–0.01 V. (b) Voltage profile of the half cell in Figure 3a. (c) Cycling performance of a half cell cycled between 1–0.1 V. (d) High rate cycling of a half cell cycled between 1–0.1 V. (e) SEM images of C–Si NWs after 5 cycles. (f) TEM images of C–Si NWs after 5 cycles.

The voltage profile the C–Si NW half cell used in Figure 3a is shown in Figure 3b. The first cycle charging (lithium alloying) has a plateau at  $\sim 0.21$  V up to 1200 mAh/g, followed by a sloping region between 0.21 and 0.01 V. This charging behavior is similar to that of amorphous Si<sup>17,23</sup> and quite different from either amorphous carbon (Supporting Information, Figure S2) or crystalline Si (plateau at  $\sim 0.11$  V).<sup>16,24</sup> This is expected since the major capacity of C–Si NWs is contributed by a-Si. After the first cycle, the charging and discharging profile shows typical behavior (sloping curves) of Li intercalating with amorphous  $\text{Li}_x\text{Si}$ .<sup>17,23</sup> The average charge potential is  $\sim 0.2$  V and average discharge potential  $\sim 0.4$  V, rendering a low average overpotential of  $\sim 0.1$  V, suggesting that silicon is a good anode material with low charge/discharge voltage hysteresis.

Previous studies have suggested that the cycling life of Si anode can be significantly improved by limiting the amount of Li intercalating with Si.<sup>24,25</sup> In Figure 3c, we cycled the C–Si core–shell NWs between 1 and 0.1 V, that is, limiting the NW voltage above 0.1 V thereby reducing the amount of Li intercalated. Rate C/15 was used for the first 2 cycles,

where the NW electrode showed a discharge capacity of 1700 mAh/g and a high first cycle efficiency of 89%. After the first 2 cycles, the charge/discharge rate was increased to C/5, where the capacity maintained a steady value of to 1300 mAh/g and coulombic efficiency was also high (98–99.6%). The rate was reduced to C/15 again after 47 cycles, whereas the capacity recovered to 1600 mAh/g. For the half cell in Figure 3c, we used the slurry spreading method to prepare the CNF film before Si deposition. The loading density of CNFs is  $\sim 0.6$  mg/cm<sup>2</sup> and after Si deposition the total active material is  $\sim 2.4$  mg/cm<sup>2</sup>. So at the rate of C/15, the C–Si NW electrode has an area capacity of  $\sim 4$  mAh/cm<sup>2</sup>, which is comparable to commercial values.

In Figure 3d, we tested another half cell at higher rates and cycled the cell between 1–0.1 V. C/5 rate was used for the first 5 cycles, then 1C for 60 cycles, and C/5 again for remaining cycles. At the high rate of 1C, the capacity remains at a large value of 800 mAh/g and the capacity was recovered to 1300 mAh/g when the rate was reduced to C/5 after 60 cycles at 1C. After a total of 80 cycles, the discharge capacity

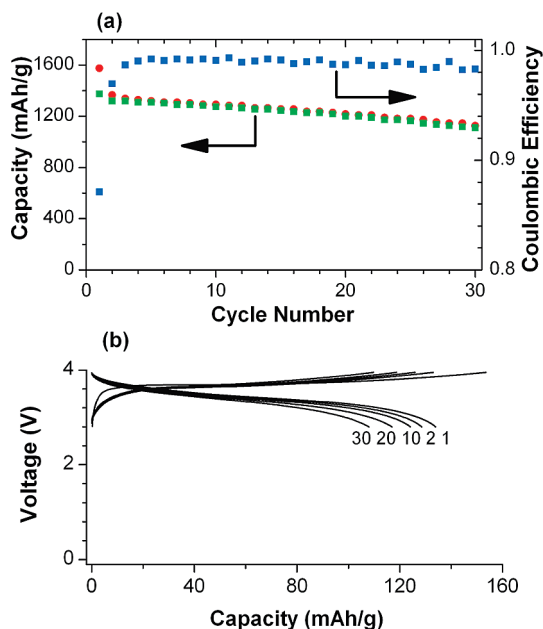


**Figure 4.** (a) Cycling performance of C–Si core–shell NWs in a LiCoO<sub>2</sub>/NW full cell, cycled between 4 and 3.5 V. (b) Voltage profile of the full cell in Figure 4a, where the specific capacity is calculated according to the weight of LiCoO<sub>2</sub>.

showed very little decay (~7%) compared to the first cycle discharge capacity.

For comparison purpose, the capacity and cycling performance of bare CNFs on a SS substrate was also investigated. Slurry made by mixing CNFs and PVdF (10% weight) in NMP was bladed on to a SS current collector to form an electrode. After drying, the CNF electrode was made into a half cell using lithium foil as counter electrode. However the cycling performance of bare CNFs is rather poor (Supporting Information, Figure S3). At rate C/5 (0.12 A/g, according to the capacity of amorphous carbon), the bare CNFs only have a reversible capacity of ~280 mAh/g and show very poor Coulombic efficiency and cycling life. This suggests that the a-Si coating greatly enhance the cycling capability of bare CNFs.

Figure 3e is a SEM image of C–Si core–shell NWs after 5 cycles (cycled between 1–0.1 V) of lithium intercalation. As we can see, the NWs still maintain good wire shapes. Figure 3f is a TEM image of a NW after 5 cycles, which no longer shows a clear core–shell structure. The repeated lithium alloying and dealloying have induced nanopore formation in Si (unpublished data) and smeared out the clear interface between carbon and silicon.

A full cell made of LiCoO<sub>2</sub> cathode and C–Si NW anode was also investigated. The mass loading density of cathode is 10 mg/cm<sup>2</sup> and C–Si NW anode about 1 mg/cm<sup>2</sup>. Figure 4a shows the cycling performance of the C–Si NW anode in the full cell. The cycling rate used is C\*/5 (1C\* = 140 mA/g) according to the specific capacity of LiCoO<sub>2</sub> cathode. In this cell, the specific capacity according to the weight of C–Si NWs is ~1400 mAh/g and the corresponding LiCoO<sub>2</sub> capacity is ~140 mAh/g. The first cycle Coulombic efficiency is 86% and following cycles around 98.5%. The full

cell has a capacity retention of 80% after 30 cycles. We believe the capacity loss during the first 30 cycles of the full cell is mainly due to the decay of LiCoO<sub>2</sub> (purchased from Sigma-Aldrich) cathode since C–Si NWs showed little fading during the first 30 cycles in half cell tests (see Figure 3a). For comparison study, we have made a cell using LiCoO<sub>2</sub> (10 mg/cm<sup>2</sup>) as cathode and Li foil as counter electrode, which also has a capacity retention of ~80% after 30 cycles (Supporting Information, Figure S4).

The voltage profile of the LiCoO<sub>2</sub>/C–Si NW full cell is shown in Figure 4b. The full cell discharges at an average voltage of ~3.3 V, which is about 0.3 V lower than commercial LiCoO<sub>2</sub>/graphite cell (~3.6 V) but still applicable. No plateau (except the first charge) was observed because C–Si NWs have a sloping voltage profile (except the first charge). The full cell has an average over potential of 0.15 V, which is as expected when counting the over potentials of both LiCoO<sub>2</sub> and C–Si NWs.

In conclusion, we have synthesized carbon–silicon core–shell NWs and obtained good battery performance using them as anodes. Since carbon has a much smaller capacity compared to silicon, the carbon core will experience less structural stress or damage during lithium cycling and can function as a mechanical support and an electron conducting pathway. These NWs have a high lithium storage capacity of ~2000 mAh/g and good cycling life. We also obtained an area capacity up to ~4 mAh/cm<sup>2</sup>, comparable to commercial values. The full cell using LiCoO<sub>2</sub> as cathode discharges at 3.3 V and is commercially applicable.

**Acknowledgment.** The work is partially supported by the Global Climate and Energy Project at Stanford, Office of Naval Research and King Abdullah University of Science and Technology (KAUST) under the Award No. KUS-11-001-12.

**Supporting Information Available:** Detailed experimental method, EDX spectra, additional TEM image, charge–discharge potential profiles, and cycling performance. This material is available free of charge via the Internet at <http://pubs.acs.org>.

## References

- (1) Obrovac, M. N.; Christensen, L. *Electrochem. Solid-State Lett.* **2004**, *7* (5), A93–A96.
- (2) Kasavajjula, U.; Wang, C. S.; Appleby, A. J. *J. Power Sources* **2007**, *163* (2), 1003–1039.
- (3) Green, M.; Fielder, E.; Scrosati, B.; Wachtler, M.; Moreno, J. S. *Electrochem. Solid-State Lett.* **2003**, *6* (5), A75–A79.
- (4) Li, H.; Huang, X. J.; Chen, L. Q.; Zhou, G. W.; Zhang, Z.; Yu, D. P.; Mo, Y. J.; Pei, N. *Solid State Ionics* **2000**, *135* (1–4), 181–191.
- (5) Zhang, X. W.; Patil, P. K.; Wang, C. S.; Appleby, A. J.; Little, F. E.; Cocke, D. L. *J. Power Sources* **2004**, *125* (2), 206–213.
- (6) Liu, W. R.; Guo, Z. Z.; Young, W. S.; Shieh, D. T.; Wu, H. C.; Yang, M. H.; Wu, N. L. *J. Power Sources* **2005**, *140* (1), 139–144.
- (7) Zhang, T.; Gao, J.; Zhang, H. P.; Yang, L. C.; Wu, Y. P.; Wu, H. Q. *Electrochem. Commun.* **2007**, *9* (5), 886–890.
- (8) Mao, O.; Turner, R. L.; Courtney, I. A.; Fredericksen, B. D.; Buckett, M. I.; Krause, L. J.; Dahn, J. R. *Electrochem. Solid-State Lett.* **1999**, *2* (1), 3–5.
- (9) Mao, O.; Dunlap, R. A.; Dahn, J. R. *J. Electrochem. Soc.* **1999**, *146* (2), 405–413.
- (10) Kim, I.; Kumta, P. N.; Blomgren, G. E. *Electrochem. Solid-State Lett.* **2000**, *3* (11), 493–496.
- (11) Kim, I. S.; Kumta, P. N. *J. Power Sources* **2004**, *136* (1), 145–149.

- (12) Yoshio, M.; Kugino, S.; Dimov, N. *J. Power Sources* **2006**, *153* (2), 375–379.
- (13) Yang, J.; Wang, B. F.; Wang, K.; Liu, Y.; Xie, J. Y.; Wen, Z. S. *Electrochem. Solid-State Lett.* **2003**, *6* (8), A154–A156.
- (14) Lee, H. Y.; Lee, S. M. *J. Power Sources* **2002**, *112* (2).
- (15) Kim, B. C.; Uono, H.; Satou, T.; Fuse, T.; Ishihara, T.; Ue, M.; Senna, M. *J. Electrochem. Soc.* **2005**, *152* (3), A523–A526.
- (16) Chan, C. K.; Peng, H. L.; Liu, G.; McIlwrath, K.; Zhang, X. F.; Huggins, R. A.; Cui, Y. *Nat. Nanotechnol.* **2008**, *3*, 31–35.
- (17) Cui, L. F.; Ruffo, R.; Chan, C. K.; Peng, H. L.; Cui, Y. *Nano Lett.* **2009**, *9* (1), 491–495.
- (18) Chan, C. K.; Zhang, X. F.; Cui, Y. *Nano Lett.* **2008**, *8*, 307–309.
- (19) Chan, C. K.; Ruffo, R.; Hong, S. S.; Huggins, R. A.; Cui, Y. *J. Power Sources* **2009**, *189* (1), 34–39.
- (20) Chan, C. K.; Ruffo, R.; Hong, S. S.; Cui, Y. *J. Power Sources* **2009**, *189* (2), 1132–1140.
- (21) Kim, H.; Cho, J. *Nano Lett.* **2008**, *8* (11), 3688–3691.
- (22) Peng, K.; Jie, J.; Zhang, W.; Lee, S. T. *Appl. Phys. Lett.* **2008**, *93*, (3).
- (23) Maranchi, J. P.; Hepp, A. F.; Kumta, P. N. *Electrochem. Solid-State Lett.* **2003**, *6* (9), A198–A201.
- (24) Obrovac, M. N.; Krause, L. J. *J. Electrochem. Soc.* **2007**, *154* (2), A103–A108.
- (25) Liu, W. R.; Yang, M. H.; Wu, H. C.; Chiao, S. M.; Wu, N. L. *Electrochem. Solid-State Lett.* **2005**, *8* (2), A100–A103.

NL901670T